Acta Cryst. (1996). D**52**, 785–798

Repartitioning of NaCl and Protein Impurities in Lysozyme Crystallization

PETER G. VEKILOV,[a] LISA A. MONACO,[a] BILL R. THOMAS,[a] VIVIAN STOJANOFF[b] AND FRANZ ROSENBERGER[a]

[a]*Center for Microgravity and Materials Research, University of Alabama in Huntsville, Huntsville, Alabama 35899, USA, and* [b]*Biology Department, Brookhaven National Laboratory, Upton, New York 11973, USA. E-mail: peter@cmmr.uah.edu*

(Received 7 November 1995; accepted 5 March 1996)

Abstract

Nonuniform precipitant and impurity incorporation in protein crystals can cause lattice strain and, thus, possibly decrease the X-ray diffraction resolution. To address this issue, a series of crystallization experiments were carried out, in which initial supersaturation, NaCl concentration, protein purity level and crystallized fraction were varied. Lysozyme and protein impurities, as well as sodium and chloride were independently determined in the initial solution, supernatant and crystals. The segregation coefficients for Na^+ and Cl^- were found to be independent of supersaturation and NaCl concentration, and decreased with crystallized fraction/crystal size. Numerical evaluation of the extensive body of data, based on a nucleation–growth–repartitioning model, suggests a core of $\sim 40\,\mu m$ in which salt is incorporated in much greater concentrations than during later growth. Small crystals containing higher amounts of incorporated NaCl also had higher protein impurity contents. This suggests that the excess salt is associated with the protein impurities in the core. X-ray topography revealed strain fields in the center of the crystals comparable in size to the inferred core. The growth rates of crystals smaller than 30–40 μm in size were consistently 1.5–2 times lower than those of larger crystals, presumably due to higher chemical potentials in the core.

1. Introduction

Strain and defects in crystals often arise from the nonuniform chemical composition that results from nonsteady repartitioning of precipitant and impurities during crystallization. Since this may limit the obtainable X-ray diffraction resolution, an understanding of repartitioning phenomena should be of concern in the pursuit of protein crystal perfection.

The channels between the macro-ions in protein crystals are lined with protein-bound (ordered) water (Frey, 1994; Madhusudan, Kodandapani & Vijayan, 1993) and possibly some regularly arranged precipitant ions (Blake, Mair, North, Phillips & Sarma, 1967). Hence, contrary to widespread belief, it is thermodynamically unlikely that the solution composition in the channels is the same as that of the bulk solution from which a crystal grows. As a consequence, one might expect considerable repartitioning at the crystal–solution interface (Rosenberger, 1986). In addition, impurities, including other proteins, may either be (partly) rejected, or incorporated into the crystals.

Traditionally, estimates of the amounts of precipitant ions incorporated into protein crystals have been based on mere crystallographic considerations. For instance, one could expect that the ions per molecule equal the number of charges or basic groups on the protein molecule. For hen egg-white lysozyme, at $pH = 4.5$, these are 12 (Tanford & Wagner, 1954; Tanford, 1962; Roxby & Tanford, 1971) and 19 (Blake *et al.*, 1965), respectively. However, under quasi-equilibrium conditions, that is low enough growth rates, the repartitioning of components is governed by their chemical potential differences between solution and crystals. Therefore, precipitant and impurity concentrations in the crystals should increase with their concentration in the solution. Furthermore, under nonequilibrium conditions, that is at higher growth rates, precipitant and impurity incorporation may be reduced due to transport limitations (Rosenberger, 1986), or either increased or decreased for kinetic reasons (trapping, adsorption-limitation, *etc.*) (Chernov, 1984). Thus, either variations in growth rate or different adsorption behavior of different crystal faces can result in nonuniform precipitant and impurity incorporation. Such considerations are commonplace for inorganic materials. On the other hand, the diffusivities of numerous species in globular protein crystals are high enough, for, *e.g.*, the post-crystallization preparation of heavy-metal derivatives. Hence, one might expect that nonuniform distributions from repartitioning may readily be equalized after growth.

Precipitant repartitioning has only been studied by a few investigators. In pioneering work (Elgersma, Ataka & Katsura, 1992) the residual Cl^- concentrations in the supernatant in lysozyme crystallization were measured. The authors concluded that precipitant is incorporated into the crystals in significant amounts. Sibille & Pusey, (1994) measured the heat of mixing of NaCl and lysozyme solutions, and interpreted their results in terms of association between the protein and Cl^- in the

solution. Although such phenomena are typically discussed in terms of the ionicity of the precipitants, recent light scattering studies of the nonideal behavior in lysozyme solutions containing NaCl or $NaOOCCH_3$ revealed pronounced salt-specific effects (Muschol & Rosenberger, 1995).

Hence, the purpose of our study was to investigate the repartitioning of the precipitant ions, Na^+ and Cl^-, under different lysozyme crystallization conditions. The main conclusions to be drawn from this work are that the incorporation of the precipitant is coupled to protein impurities incorporation, and that both impurities and precipitant accumulate in the center of crystals, thus forming a core. We provide X-ray topography results that reveal lattice strain associated with this coring. Finally, growth rates in the core-formation stages will be shown to be consistently lower than for larger crystal sizes, presumably because of a higher chemical potential in the core region.

2. Experimental procedures

Four grades of lysozyme were used as supplied by (i) Sigma or (ii) Seikagaku, (iii) Seikagaku stock purified by ion-exchange liquid chromatography, and (iv) grade (iii) contaminated with 4%(*w/v*) avidin. Solutions of the as-received preparations were prepared as described by Rosenberger, Howard, Sowers & Nyce (1993). The protein impurity analysis and purification procedures were as described by Thomas, Vekilov & Rosenberger (1996) and Rosenberger, Vekilov, Muschol & Thomas (1996).

Crystallization experiments were carried out at 277 K in test tubes containing 5 or 10 ml of solution. The smaller volumes were used in experiments with the scarce purified material, and in control runs with Sigma and Seikagaku lysozyme. These controls showed no influence of the solution volume over this range. In all experiments, pH = 4.5 (50 m*M* sodium acetate buffer) and 2.5 or 5%(*w/v*) NaCl precipitant were used. Lysozyme concentrations were varied from 8 to 50 mg ml^{-1}. Hence, depending on the specific experiment, the ratio of ions to lysozyme molecules in the solution ranged from 780 to 120.

Supersaturations were calculated as $\sigma = \ln(C/C_{sat})$. At 277 K the lysozyme solubility at 2.5% NaCl is $C_{sat} = 2$ mg ml^{-1}, as determined in a 3 months batch crystallization experiment. This value can also be interpolated from data for 2 and 3% NaCl (Cacioppo & Pusey, 1991), and other data obtained in our group (Rosenberger *et al.*, 1993). At 5% NaCl, the experiments had to be performed at 291 K, since amorphous precipitate formed at 277 K. Under these conditions, the lysozyme solubility is $C_{sat} = 1.8$ (Cacioppo & Pusey, 1991).

The supernatant was separated from the crystals by filtration through 5 μm pore size filters. Most of the crystals remained attached to the test tube walls, the remainder were retained by the filter. The crystals were well faceted, with the typical tetragonal lysozyme habit. They were predominantly found on the lower tube walls, indicating nucleation mostly in the bulk solution, followed by sedimentation. The number and size of crystals was estimated for each tube. Depending on initial supersaturation, the number of crystals was of the order 10^3–10^4. At lysozyme concentrations < 20 mg ml^{-1}, the crystals were well separated, so no solution was trapped between them. To prevent solution adhering to the surface of the crystals or tube walls causing bias in our measurements, we rinsed the crystals on the walls and on the filter with 1 ml deionized water at 277 K. This caused slight etching, as revealed by microscopic observation. The rinsing water was added to the supernatant. The filter was then transferred into the test tube and the crystals were dissolved in 5 or 10 ml deionized water.

The lysozyme, precipitant ions and, in some cases, protein impurity amounts were determined in the initial solution, the supernatant and in the dissolved crystals. It should be emphasized that these quantities in the crystals were directly determined, rather than as differences between the concentrations in the initial and supernatant solutions. This allowed us to obtain reproducible results with crystallized fractions as low as 3–4%. As will be seen below, most of the novel phenomena were observed in experiments where less than 10% of the initial lysozyme in the solution was crystallized.

The lysozyme concentrations were determined by UV spectrophotometry, using $\alpha^{280nm} = 2.64$ ml mg^{-1} cm^{-1} (Sophianopoulos, Rhodes, Holcomb & Van Holde, 1962). The Na^+ concentrations were measured with an atomic absorption (AA) spectrometer, which was zeroed and calibrated with dH_2O and 1 mg l^{-1} Na^+ standard, respectively. After each series of measurements, the stability of the readings was checked and, if necessary, the samples were remeasured. Since the advantageous concentration range for Na^+ determinations is 0.3–1.3 mg l^{-1}, the initial and supernatant solutions were diluted 10 000-fold, and the solutions containing dissolved crystals 20- to 200-fold. The Cl^- concentrations were determined by ion selective potentiometry. Since protein in the solution damages the electrode, the lysozyme was separated from the sample by ultrafiltration prior to the analysis. For this, 400 μl of solution were placed in a centrifugal ultrafilter with *MW* cutoff at 5–6000 kDa, and spun on a mini-centrifuge at ~2000*g* for ~40–60 min. Before each series of potentiometric measurements a new standard curve was obtained for the Cl^- probe. Variations in this curve remained below 5% if the same electrode was used. Each determination was bracketed by standard measurements to verify probe stability and was repeated three or four times. Protein

Table 1. *Comparison of ion incorporation and segregation coefficients for two NaCl concentrations and three initial lysozyme concentrations*

Since n^{crys} and k strongly depend on the crystallized fraction, only comparison between measurements of equal crystallized fractions are meaningful. Note that although the n^{crys} is about twice as high in 5% NaCl solution as in the 2.5% NaCl solution, the k values are very close.

	5% NaCl 291 K			2.5% NaCl 277 K		
C^0_{lys} (mg ml^{-1})	14.9	19.9	37.1	18.0	18.0	38
σ_0	2.1	2.4	3.1	2.2	2.2	3.0
n^{soln}	830	630	340	340	340	164
Crystallized fraction	0.16	0.11	0.09	0.16	0.11	0.09
$n^{crys}_{Na^+}$	18.5	26.7	20.4	8	13	10
$n^{crys}_{Cl^-}$	15	22.6	15.1	6	9	7
k_{Na^+}	0.022	0.041	0.060	0.023	0.038	0.061
k_{Cl^-}	0.018	0.036	0.045	0.017	0.026	0.042

composition analysis was performed by sodium dodecyl sulfate polyacrylamide gel electrophoresis (SDS-PAGE) with silver staining as described by Thomas *et al.* (1996).

Each series consisted of two to three experiments if purified lysozyme was used, or five to six experiments in the other cases. Within a series, either the initial lysozyme concentration or crystallized fraction of lysozyme were varied. Each series was repeated at least once. The investigation of the time-dependence of salt incorporation for 18 mg ml^{-1} Sigma lysozyme solutions was performed five times. The results for the separate experimental series were very consistent.

To estimate a possible systematic error in our lysozyme and the precipitant ion determinations, especially when small crystal quantities were analyzed, we performed two control experiments. One test tube containing 10 ml of deionized water and another one with 11 mg ml^{-1} lysozyme solution with buffer and precipitant, were kept at 277 K for several hours, so that no crystals formed in the second tube (compare with crystallization kinetics curves in §3). Then the contents of both tubes were analyzed for lysozyme, Na^+ and Cl^- following the full procedure described above, including filtration and rinsing. The results obtained for the processed pure water sample indicated no salt or protein pickup in our procedure. In the second control experiment, we found that 0.2 mg of lysozyme and 0.7 mmol of NaCl apparently adhered to the tube walls or the filter even after rinsing. Hence, even with the smallest amount of crystals analyzed in our experiments (3.4 mg or 0.25 mmol), the systematic error in the determination of the crystallized lysozyme amount could only be +6%, and in the number of ions per lysozyme molecule +3.

The results of Cl^- were lower than those for Na^+ in most of the determinations. To address this, we carefully tested and compared the measurement techniques for the two ions by analyzing solutions with salt/protein molar ratios and concentrations covering the range of our experiments. In ~10% of all cases, the AA measurements yielded up to 5–10% excess of Na^+, apparently picked up during the successive dilutions. Thus, all Na^+ measurements were carried out at least three times, and, if any of them was higher, the dilutions and the measurement were redone. The tests for Cl^- revealed that, independent of ion or lysozyme concentration, in the presence of protein, between ~5 and 20% of Cl^-, are unaccounted for in the filtered volume. Most likely, this is because of gradual clogging of the membrane by lysozyme, that inevitably lead to the retention of ~150–200 µl solution above the membrane. It is also possible that part of the chloride is associated with lysozyme in the solution (Sibille & Pusey, 1994).

3. Segregation of Na^+ and Cl^-

The repartitioning results of Na^+ and Cl^- ions were expressed as molecular numbers ratios $n = N^{ion}/N^{lys}$ found in the crystal, and the supernatant and the initial solutions. We also calculated effective segregation coefficients $k = n^{crys}/n^{soln} = (N^{ion}/N^{lys})^{crys}/(N^{ion}/N^{lys})^{soln}$.

In the first series of experiments, employing solutions with 2.5%(w/v) NaCl, the crystals were separated from the supernatant after between 3 and 10% of the protein had crystallized. This ensured that the supersaturation remained almost constant throughout the duration of crystallization. The measured dependence of n^{crys} on supersaturation is shown in Fig. 1(*a*). One can see that:

(*a*) at low supersaturations $n^{crys} \simeq 100$. This is much higher than one would expect from the considerations present in the *Introduction*. Since the crystals were thoroughly rinsed (see *Experimental procedures*), these high values cannot be due to solution adhering to the crystals.

(*b*) At high supersaturations, n^{crys} is much lower than at low supersaturations.

(*c*) The reproducibility of the experimental data for both ions is somewhat lower than expected from the standard deviations of the analytical methods employed. This, as we will see below, results from a dependence of n^{crys} on the fraction of lysozyme crystallized.

However, as shown by Fig. 1(*b*), on replotting these data in terms of $k(\sigma)$ one finds that the segregation coefficient, independent of supersaturation, is $k \simeq 0.1$. If n^{crys} were determined by crystallographic factors, such as number of suitable positions for salt inclusion in the lattice, or by the number of ions associated with the lysozyme molecule in the solution, we would expect constant n^{crys} and increasing k with decreasing n^{soln}. Hence, it appears that the amount of precipitant ions incorporated by the lysozyme crystals is largely determined by the ratio of ions to protein molecules in the solution.

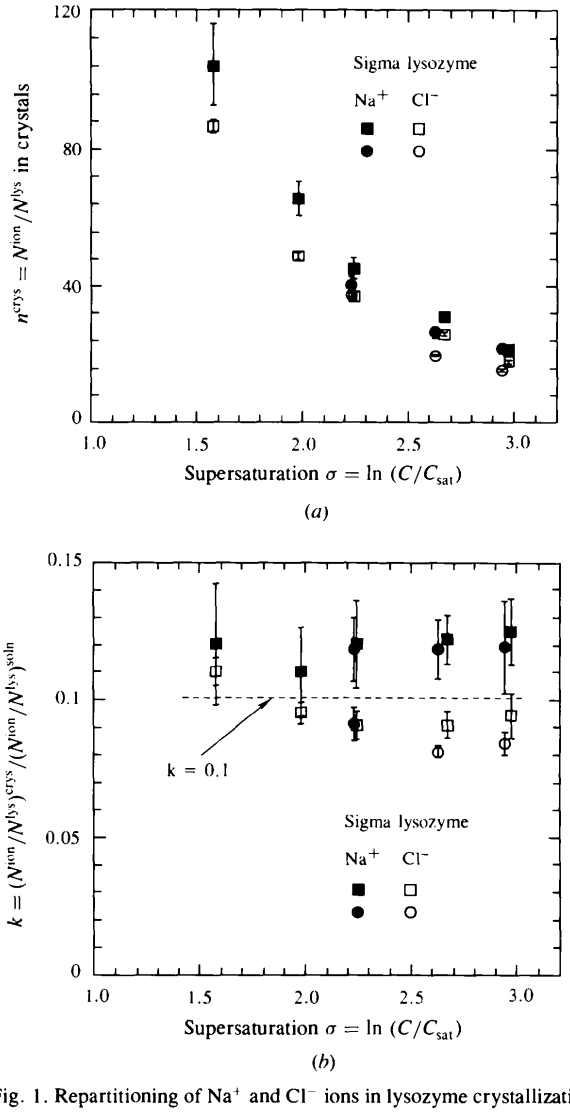

Fig. 1. Repartitioning of Na^+ and Cl^- ions in lysozyme crystallization as functions of supersaturation σ. Sigma lysozyme, 2.5% NaCl, two independent experimental series. Crystallized fractions between 3 and 10% to ensure constant supersaturation during crystallization for each point. Error bars represent the standard deviation of the measurement and do not account for systematic shifts, see §2. (*a*) Number of ions of per lysozyme molecule in the crystals, n^{crys}. (*b*) Segregation coefficient k.

To check the above conclusion, we performed experiments with a doubled NaCl concentration [5%(*w*/*v*)] and, thus, a doubled ratio of ions to lysozyme molecules in the solution. The experiments were carried out with initial C_{lys} of 14.9, 19.9 and 37.1 mg ml^{-1}. Thus, as shown in Table 1, the initial supersaturations were slightly higher than in the series with 2.5% NaCl solutions at 277 K. Table 1 also shows that the resulting n^{crys} values essentially double with the salt concentration in the solution. However, as one would expect from equilibrium arguments, the k values remained essentially the same.

To explore whether n^{crys} depends on the crystallized fraction, we performed experiments in which several crystallization tubes in a series were charged with identical solutions, but the crystallization in the tubes was terminated at individually increasing times. This added a time axis perpendicular to the (n^{crys}, σ) plane in Fig. 1(*a*). Such experimental series were carried out with three initial supersaturations, $\sigma_0 = 1.8$, 2.2 and 3.0, resulting in a three-dimensional plot of ion incorporation as a function of initial supersaturation and time. Note that, in these time series, the supersaturation dropped continuously on account of the increased crystallized fraction, and the size of the analyzed crystals increased

The results obtained from these three series are plotted in Fig. 2(*a*) as a function of the supersaturation at the separation of the crystals, σ_{sep}. Note that for each data point, the crystals grew at decreasing supersaturations between σ_0 of the series and σ_{sep}. The number of crystals in each series typically increased only insignificantly with crystallization time. This indicates that most nucleation events occurred during the early stages of crystallization, and that the crystallized fraction of lysozyme mostly increased because of the growth of these nuclei. The n^{crys} values around σ_0 agree with the values of Fig. 1(*a*) at the same supersaturation. Then n^{crys} drops sharply with σ_{sep}, approaching approximately ten times lower values at long crystallization times. Although not discussed by the authors, an analogous trend can be seen in earlier experiments (Elgersma, Ataka & Katsura, 1992). This strong dependence of n^{crys} on the crystallized fraction is likely to be the reason for the limited reproducibility of the data in Fig. 1(*a*). Note that the three data groups do not coincide in the overlapping regions of supersaturation. This demonstrates clearly that the decrease in ion incorporation is not simply following the decrease in supersaturation.

The decrease of n^{crys} with crystallization time could be because of the diffusion of captured ions back into solution. To check this hypothesis, we carried out experiments with ten tubes containing the same initial $C_{lys} = 18$ mg ml^{-1}, *i.e.* $\sigma_0 = 2.2$. Tubes were removed from the refrigerator in pairs at increasing times. Each time, the crystals and solution in one of the tubes were

analyzed immediately. However, the second tube was placed for 6 d into an incubator at saturation temperature, and only then were the crystals analyzed. We found that there is essentially no difference between n^{crys} obtained from the two sets of tubes. Hence, the results are plotted together in Fig. 2(*a*). Therefore, we can conclude that back-diffusion of captured precipitant ions to the solution cannot be the reason for the observed decreasing concentrations with increasing crystallization time.

Replotting of the n^{crys} data in Fig. 2(*a*) in terms of $k(\sigma_{sep})$ reveals important similarities. Fig. 2(*b*) shows that in all three series the initial and the final segregation coefficients, rather independent of supersaturation, are $k_0 = 0.1$ and $k_f = 0.003$. This strongly suggests a dependence of k on crystal size. As mentioned above, the number of crystals in a series was roughly constant and $k(\sigma_{sep})$ represents a k value averaged over all crystals formed since the beginning of crystallization. Thus, $k(\sigma_{sep})$ decreases mostly because of the growth of the existing crystals, and the precipitant incorporation in small crystals is apparently characterized by k_0 and in the outermost 'shells' by k_f. The intermediate k values are determined by the ratio of k_f to k_0 material in the crystals. Hence, with increasing crystal size k approaches k_f.

Another similarity between the three data sets is suggested by the increasing curvature of $k(\sigma_{sep})$ with decreasing σ_0 in Fig. 2(*d*). Hence, we have replotted the data in Fig. 3 in terms of the normalized supersaturation σ_{sep}/σ_0. This normalization reduces the three data sets to one. Thus, the dependence of ion incorporation on time (or σ_{sep}) is apparently also governed by σ_0. The initial supersaturation, on the other hand, is an essential parameter in the nucleation and growth kinetics underlying these repartitioning processes. Therefore, we will attempt to correlate ion incorporation to the nucleation and growth kinetics underlying the above three series of experiments.

Hence, we have plotted the measured crystallized fractions of the above triple series *versus* crystallization time in Fig. 4. In comparing these dependencies to the corresponding n^{crys} in Fig. 2(*a*), one notes that higher salt incorporation occurs in the same time span as the steep increase in the fraction crystallized. As we will show below, this exponential increase denotes the regime in which nucleation dominates over the growth of existing crystallites. Hence, we tentatively conclude that newly nucleated, small crystals capture a larger amount of precipitant per lysozyme molecule than during the ensuing growth to larger sizes. Thus, ion-rich crystal cores are surrounded by crystalline shells that have less salt. In the following section, we will show that all the above data are quantitatively compatible with results obtained from a model which combines the

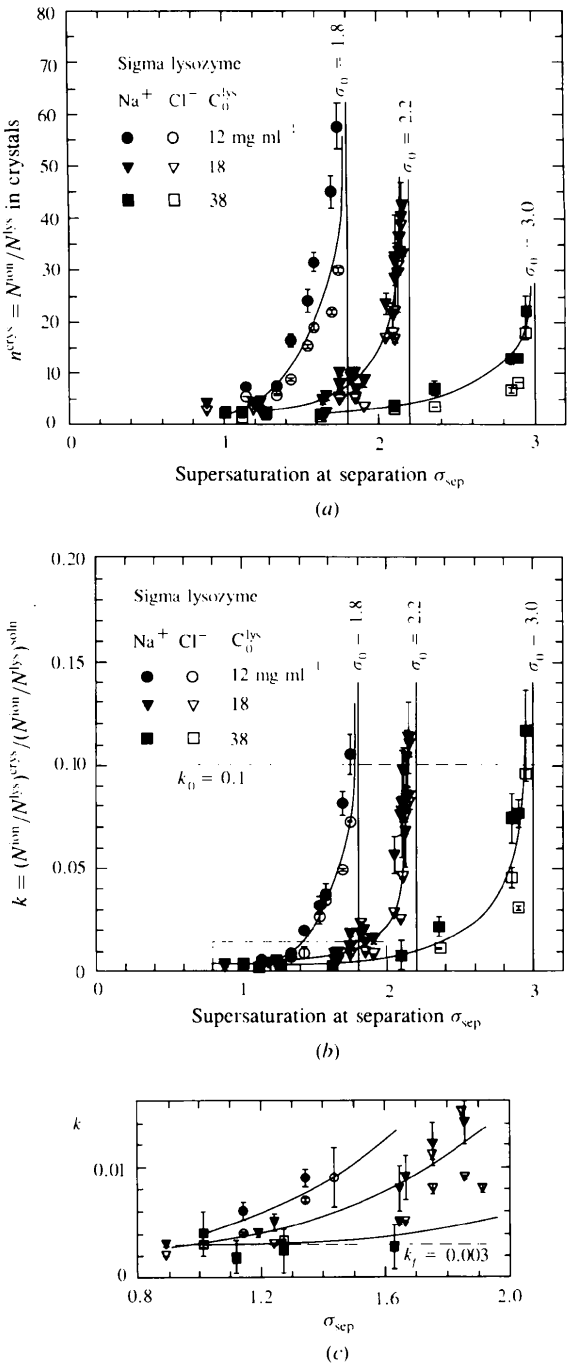

Fig. 2. Repartitioning of Na^+ and Cl^- ions in lysozyme crystallization from Sigma solutions, containing 2.5% NaCl, as functions of supersaturation at separation σ_{sep} for three initial protein concentrations/supersaturations. The crystals separated at each σ_{sep} grew at supersaturations decreasing from σ_0 (marked by vertical lines) to σ_{sep}. Error bars represent the standard deviation of the measurement and do not account for systematic shifts, see §2. Curves are just guides for the eye. (*a*) Number of ions per lysozyme molecule in the crystals, n^{crys}. (*b*) The segregation coefficient k. (*c*) Blown-up view of the area within the dashed rectangle in (*b*).

nucleation and crystal growth aspects of the experiments with the assumed formation of salt-rich cores in the crystals.

4. Nucleation-growth and salt incorporation model

4.1. *Nucleation*

Following earlier works (Kam, Shore & Feher, 1978; Feher & Kam, 1985; Boistell & Astier, 1988), the nucleation of protein crystals has been dealt with by various authors (Ataka & Asai, 1990; Elgersma *et al.*, 1992; Besho, Ataka, Asai & Katsura, 1994; Malkin, Cheung & McPherson, 1993; Malkin & McPherson, 1993*a*,*b*, 1994). Ataka and co-workers followed the dependence of the residual lysozyme concentration on time. Nucleation was postulated to proceed according to the protein self-assembly mechanism. The size of the critical nucleus was tacitly assumed to be independent of supersaturation. As a consequence, nucleation was envisioned as an unusual fourth-order chemical reaction.

In a pioneering application of the classical approach, Malkin *et al.* deduced the time dependence of the average cluster radius from quasi-elastic light scattering data. From this, critical sizes of nuclei for various proteins were estimated to contain as few as seven molecules. However, in view of modern atomistic and statistical nucleation theories (see Mutaftschiev, 1993; Kashchiev, 1995; Milchev, 1991, and references therein), the continuum approach used for these estimates should be met with reservation. Similarly, an activation energy for crystallization was estimated from the measured nucleation rate. Unfortunately, as in numerous earlier works, Malkin *et al.* used an erroneous squared (rather than linear) concentration term (Mutaftschiev, 1993) in the rate equations.

In response to the above inconsistencies, we have carefully reviewed the assumptions and results of modern nucleation theories. These considerations are summarized in the *Appendix*. We show that at the highest supersaturation employed in our experiments, the critical nucleus consists of approximately ten lysozyme molecules. Therefore, we employ a statistical-thermodynamics formulation of nucleation, mostly following a recent review by Mutaftschiev (1993), rather than a purely classical approach (Kahlweit, 1969; Chernov, 1984) that does not account for cluster motion in the solution. Furthermore, we show that, because of the slow rate of nucleation and crystal growth, the steady-state approximation is applicable to our system. In addition, we critically evaluate the spatial, frequency and energy factors specific for protein crystallization systems as they result from the solution environment, the large size of the molecules, their low surface energy, and the mostly kinetics controlled nature of the attachment processes.

The resulting relation (15) shows that the nucleation rate is linearly related to the (protein) concentration C in the form,

$$J = AC\exp(-B/\sigma^2), \tag{1}$$

with

$$A = 2\Omega(\gamma/\pi m)^{1/2} q_{\rm rep} \exp(-E_a/k_BT)K_C, \tag{2}$$

and

$$B = 16\Omega^2\gamma^3/3\pi(k_BT)^3, \tag{3}$$

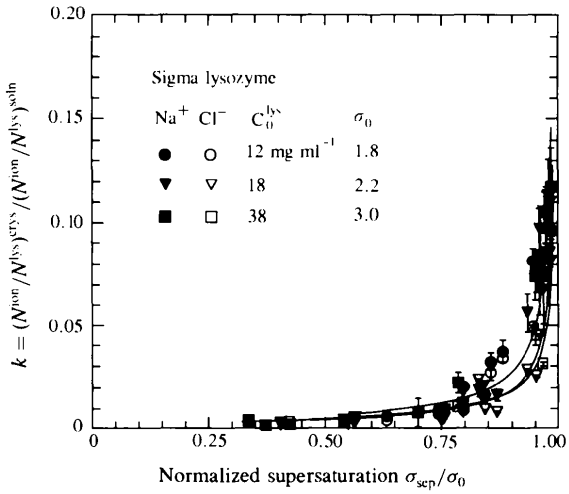

Fig. 3. Dependence of the segregation coefficient k on the supersaturation at separation normalized with respect to the initial, σ_{sep}/σ_0. Points: experimental results corresponding to those represented in Fig. 2, curves: results of the nucleation–growth–coring model with the parameters in Table 2, see §4.3.

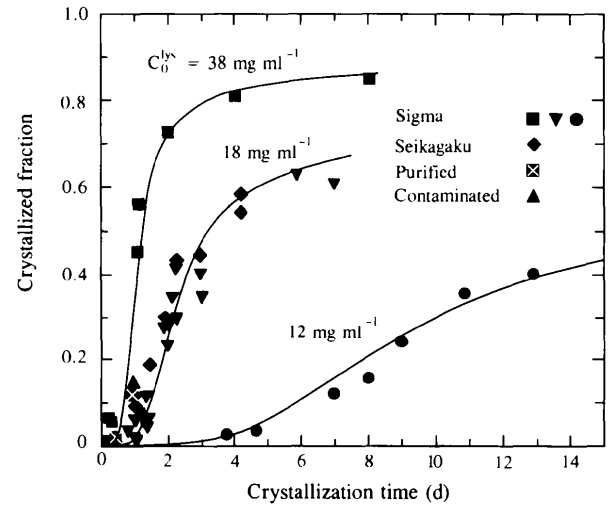

Fig. 4. Dependence of the crystallized fraction on time for three initial concentrations. Points: experimental results for four levels of lysozyme purity, Sigma data corrsponding to those represented in Figs. 2 and 3. Curves: results of the nucleation–growth model as fitted to the Sigma experimental points, with the parameters in Table 2, see §4.3.

where m and Ω are, respectively, the lysozyme molecule's mass and volume in the crystal, γ is the surface free energy of the critical cluster, E_a is the activation energy of attachment to the critical cluster, and q_{rep} is the replacement partition function of the critical cluster (see *Appendix*). $K_C = N_{Av}/(1000 \times M_{lys}) = 4.15 \times 10^{16}\,mg^{-1}$ is a conversion constant between mass concentration ($mg\,ml^{-1}$) and molar concentration units (molecules cm^{-3}), with N_{Av} and M_{lys} being Avogadro's number and lysozyme relative molecular mass, respectively.

4.2. *Growth of crystals*

Based on our previous lysozyme growth kinetics studies, we assumed that the crystal growth rate R depends on supersaturation as,

$$R = 0.26 - 1.55\sigma + 1.73\sigma^2, \quad \sigma \leq 2. \qquad (4a)$$

and

$$R = 0.16 + 2.22\sigma, \quad \sigma > 2. \qquad (4b)$$

These relations incorporate the functional form found at higher temperatures for material of the same purity (Vekilov, 1993; Monaco & Rosenberger, 1993; Vekilov & Rosenberger, 1996); the numerical values, however, were adjusted to give realistic results at 277 K used in our experiments (Vekilov, Ataka & Katsura, 1995). It should be noted that the above growth kinetics studies have shown that the lysozyme interface kinetics is much slower than transport to the interface. Hence, this system well fulfills the uniform concentration assumption underlying all above relations. For calculations of the crystallized fraction, we have assumed that growth on each nucleus occurs in the form of a cube, the linear dimensions of which are governed by the normal growth rates of (4).

4.3. *Numerical evaluation*

We evaluated the model of (1)–(4) for the three initial lysozyme concentrations of 12, 18 and 38 $mg\,ml^{-1}$ and the solution volume of 10 ml used in the time-dependence series. The experimental crystallization times were divided into 150 simulation steps. During a step, the lysozyme concentration, supersaturation, and the resulting nucleation flux and growth rate were assumed constant. The supersaturation was assumed to change from step to step only on account of lysozyme depletion, and not because of solubility changes due to the (small) salt concentration variations. In each simulation step, we calculated the number of newly nucleated crystals, as well as the lysozyme amount removed from the solution due to the growth of the existing crystals. The new supersaturation was then used to calculate the nucleation flux and the crystal growth rate in the next step *etc*. The adequacy of the time steps was checked by doubling their number, which caused only minor changes in the results.

Table 2. *Parameters determined from fitting the nucleation–growth–coring model results to the experimental data for three initial solution concentrations, as shown in Figs. 3 and 4*

Only the results for Sigma lysozme were considered. A and B are fitting coefficients, γ surface free energy of the critical cluster, q_{rep} replacement partition function for the critical cluster. For details, see text.

Initial concentration ($mg\,ml^{-1}$)	12	18	38
A ($mg^{-1}\,s^{-1}$)	1×10^{16}	1×10^{16}	1×10^{16}
B	147	203	357
γ ($mJ\,m^{-2}$)	0.81	0.90	1.09
q_{rep} (cm^{-3})	6.6×10^{12}	6.6×10^{12}	6.6×10^{12}
Maximal crystal size (μm)	340	160	85
Core size (μm)	52	26	23

Since reliable values of the parameters γ and E_a, that govern the nucleation of lysozyme are not available, we fitted the theoretical dependence of the crystallized amount on time resulting from (1)–(4) to the three sets of experimental data in Fig. 4 and, thus, determined the parameters A and B in (1); see Table 2. The pre-exponential terms A are the same for all three series. Using this A value, the replacement factor q_{rep} was calculated from (2) assuming $E_a = 20\,kJ\,mol^{-1}$ (see *Appendix*). Theoretical and experimental estimates of the q_{rep} have yielded results in the range 10^3–10^{25} (Lothe & Pound, 1969). Larger values are usually interpreted as evidence of the importance of the statistical-thermodynamic contributions to the energy of cluster formation. Thus, it appears that these contributions are also important for our system, in which the critical clusters can consist of as few as ten molecules. Also note that the values of q_{rep} are quite different to the values of the monomer concentration in our and other crystallizing protein systems, $n_l = CN_{Av}/1000\,M_{lys}$, is typically of order 10^{18}. Thus, if instead of (1) we had used the classical expression that does not account for q_{rep}, but has C^2 instead of C (Katz, 1970; Katz & Ostermier, 1967; Kahlweit, 1969; Chernov, 1984; Malkin & McPherson, 1994), questionable estimates of the nucleation and growth parameters would have been obtained.

In contrast to the constant A values, the fits resulted in a systematic variation in B. The corresponding slight increase in the values of γ with initial concentration (see Table 2) implies higher barriers for nucleation at the higher supersaturation, *i.e.* at smaller critical sizes. However, the homogeneous nucleation theories predict only lower nucleation barriers for smaller clusters, by either invoking a lower γ (Tolman, 1949) or higher energy gains from the translational and rotational degrees of freedom (Lothe & Pound, 1962). Hence, as a possible explanation for the observed tendency in γ, we assume a certain initial concentration of centers for

heterogeneous nucleation (dust or/and large-molecule impurity particles). A heterogeneous reduction of nucleation barriers is relatively more important at lower supersaturations. Indeed, our studies of the couple impurity/precipitant repartitioning, §6, indicate that the intake of the high *MW* impurities is much higher for small crystals. Thus, it is conceivable that these protein impurities act as heterogeneous nucleation centers.

The model curves obtained for the crystallized fraction are shown in Fig. 4. They are in good agreement with the experimental points for Sigma lysozyme. We also calculated the average and maximal size of the crystals at different stages of crystallization, see Table 2. The calculated sizes agree well with the observed ones. The good correspondence between the numerical and experimental results supports the applicability of this nucleation and growth model to our system.

4.4. *Simulation of salt incorporation*

In the simulations of the Na^+ and Cl^- ions incorporation we simplified matters by assuming that each lysozyme molecule enters the crystal with the same number N of both ions. To account for the suspected coring, N for freshly formed crystals, N_0, was assumed to be larger than that for large crystals, N_f. The values of N_0 and N_f were obtained for each initial supersaturation by multiplying the respective n^{soln} by $k_0 = 0.01$ and $k_f = 0.003$. The drop from N_0 to N_f was assumed to follow a specific functional dependency until a crystal reached a size $2L_c$. In each simulation step, we updated the quantity of ions and lysozyme in the solution and growing crystal to obtain average values for n^{crys} and segregation coefficients k.

We used various combinations of L_c values and functional dependencies for the drop from N_0 to N_f on crystal size. Best agreement with the experimental data in Fig. 3 was obtained with an exponential dependence and L_c values shown in Table 2, which lead to the three curves in Fig. 3. The good agreement between the experimental and modelling results gives credence to our coring hypothesis.

5. Further evidence for coring

For further tests of the coring hypothesis, we performed a set of experiments with seeded and unseeded solutions with $C^0_{lys} = 12\,mg\,ml^{-1}$. As seeds we used crystallites formed in a $50\,mg\,ml^{-1}$ solution, which according to the trend represented by Figs. 1 and 2, possess low ion contents even in the core. In four seeded tubes, up to 70% of the protein crystallized in 2 d. In the unseeded tubes, crystals appeared only after 3 d. The results obtained for various crystallized fractions are shown in Fig. 5. In the seeded solutions n^{crys} remained essentially independent of crystal size, *i.e.* of σ_{sep}/σ_0. The unseeded runs show again the initial high incorporation, dropping with time (decreasing σ_{sep}/σ_0) to the same value as in the seeded runs. Hence, with the introduction of low-salt seeds, the formation of the salt-rich cores, typical for the low supersaturations used, was apparently suppressed.

Recently, there have been numerous discussions of the presence of aggregates in crystallizing lysozyme solutions, that were even envisioned as building blocks in crystallization (Pusey, 1992; Wilson & Pusey, 1992; Niimura, Minezaki, Ataka & Katsura, 1994; Nadarajah, Forsythe & Pusey, 1995). It is feasible that larger aggregates will associate with fewer ions/molecules since some of the possible binding sites may take part in protein–protein contacts. In this way, higher concentrations of larger aggregates that might form at later crystallization stages could lead to larger ensembles entering the crystal and, thus, to a decrease in n^{crys}, either with time or increasing supersaturation. Along this line, we would expect less salt incorporation in the unseeded experiments since there crystals grew from older solutions. Hence, the results presented in Fig. 5 do not support this mechanism.

6. Repartitioning of impurities

Similar to the above conclusion, regions of higher contents of a foreign component have been detected in the centers of some small-molecule organic crystals (Roberts, Sherwood & Stewart, 1990; Narang, Sherwood, Cliff & Jones, 1978). The impurity molecules were shown to take part in nucleation, and to cause increased lattice strain. However, in our system, because of the small size of the precipitant ions, it is difficult to envisage a direct influence on lattice

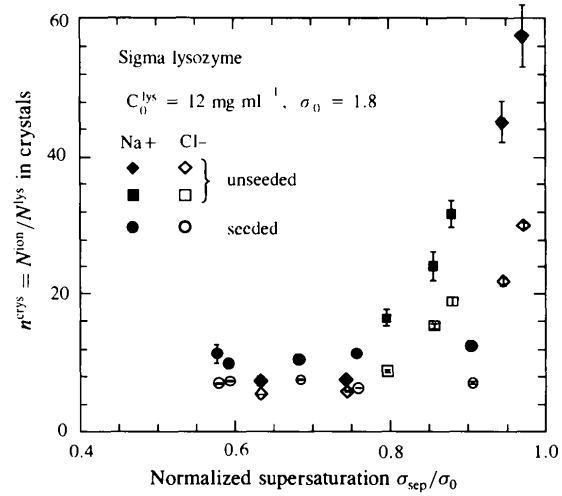

Fig. 5. Comparison between ions incorporation in seeded and unseeded crystallization, two independent unseeded series.

perfection. On the other hand, our parallel investigations have shown that higher *MW* protein impurities are present in Sigma lysozyme in weight-percent quantities (Thomas, Vekilov & Rosenberger, 1996; Rosenberger *et al.*, 1996). We have also shown that these large impurities affect growth morphology and kinetics, and are selectivity segregated during growth (Vekilov, Monaco & Rosenberger, 1995; Vekilov & Rosenberger, 1996). Thus, it is feasible that the salt-rich core is formed by the accumulation of other protein species, which, in turn, are associated with higher numbers of salt ions.

To verify whether salt repartitioning might be related to protein impurity incorporation, we carried out experiments with lysozyme solution at four different purity levels. Fig. 6 shows that the magnitude of the initial salt uptake depends on the concentration of protein impurities. The n^{crys} values at the smaller crystallized fractions obtained from the purer Seikagaku solutions are lower, and drop even further on crystallization from purified solution. However, on addition of avidin to the purified material, the n^{crys} for small crystals were as high as for the Sigma lysozyme. Fig. 7 shows that, in growth from the contaminated solutions, the avidin incorporation decreases with crystallized fraction in analogy to the salt incorporation shown in Fig. 6. Furthermore, the ion incorporation in crystals grown from purified material is always low. Thus, this series of experiments unambiguously correlates the enhanced salt uptake in small crystals to the preferential incorporation of protein impurities.

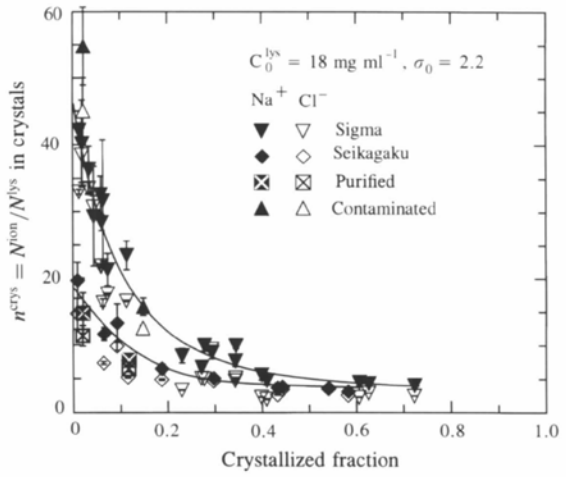

Fig. 6. Numbers of Na^+ and Cl^- ions per lysozyme molecule in the crystals, n^{crys}, as functions of crystallized fraction, for four solution purity levels: as supplied Sigma, and Seikagaku material, Seikagaku purified as described in (Thomas *et al.*, 1996), and purified lysozyme with intentionally added avidin at 4% (*w/w* with respect to dry lysozyme). Curves are just guides for the eye. Note that n^{crys} decreases with crystallized fraction, and is lower for the higher purity materials.

In another series of experiments with purified and contaminated lysozyme, initial nucleation was abundant: the number of crystals formed was by an order of magnitude higher than in the other series. Filtering through a 0.22 μm filter reduced the nucleation rate in repeated experiments to values comparable to the ones discussed in §3. Thus, the reason for the excessive nucleation is probably particulate matter present in the solution. Because of the rapid drop in supersaturation due to the growth of the numerous crystals, they were several times smaller than in other experiments with

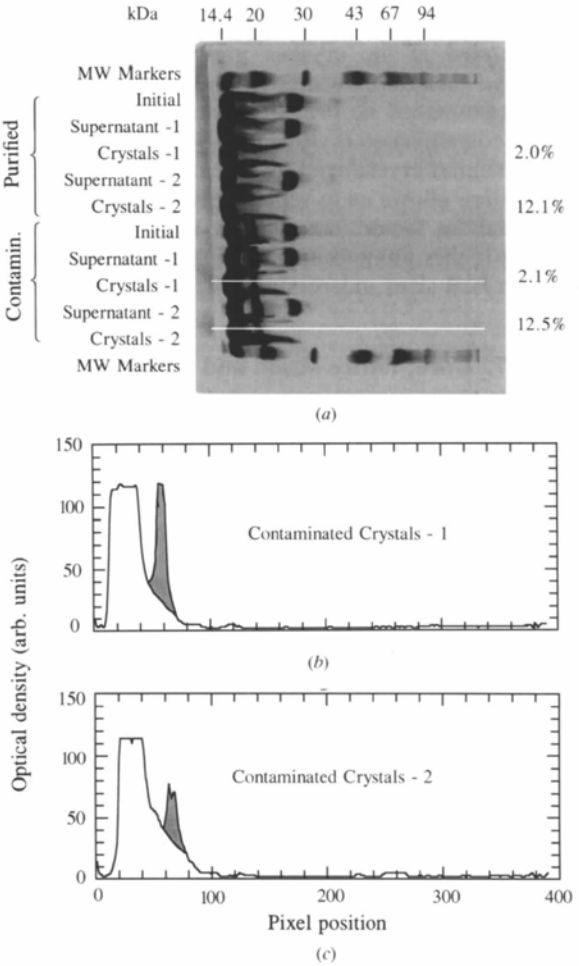

Fig. 7. Repartitioning of protein impurities during HEWL crystallization. (*a*) SDS-PAGE (12.5%), silver stained, of initial solutions, supernatant and dissolved crystals. Migration direction from right to left. Each lane loaded with ~10 μg of protein. Bands at $MW \simeq 14$, 18 and 28 kDa represent lysozyme, avidin monomer, and lysozyme dimer, respectively. Note that the dimer is preferentially rejected by the crystals. Fraction of protein crystallized upon removal of crystals is indicated on the right. (*b*) and (*c*) Optical density along lines in (*a*). Avidin concentrations in the respective dissolved crystals are roughly proportional to the gray areas in (*b*) and (*c*). At the higher fraction crystallized (case 2) the avidin incorporation in the contaminated crystals is lower, as is the corresponding precipitant ion incorporation, see Fig. 6.

Table 3. *Comparison of the incorporation of Na^+ and Cl^- in the crystals from purified and intentionally contaminated solutions in the experimental series with higher nucleation rate*

	Purified			Contaminated		
	Crystallized fraction	$n^{crys}_{Na^+}$	$n^{crys}_{Cl^-}$	Crystallized fraction	$n^{crys}_{Na^+}$	$n^{crys}_{Cl^-}$
1	0.30	7.6	4.7	0.39	14.9	9.4
2	0.36	5.8	3.9	0.43	9.4	6.7
3	0.56	4.0	3.1	0.59	5.7	4.7

comparable crystallized fraction. Precipitant ion incorporation for these experiments is summarized in Table 3. The ion content in the contaminated crystals is considerably higher than in the purified crystals. SDS–PAGE (gels not shown) revealed that avidin was incorporated in the crystals growing from the contaminated solution, while in purified solution, the crystals contained no protein impurities. Further, n^{crys} for the contaminated crystals is also significantly higher than at similar crystallized fractions in Fig. 6. The latter observation allows us to separate the size from number of crystals as factors determining core formation. We see that higher ion and impurity incorporation exists at small crystal sizes independent of crystallized fraction.

7. Core, lattice strain and growth rate

To establish if the core induces lattice strain in the lysozyme crystals, white-beam X-ray topographs were taken of crystals especially grown for this purpose in X-ray capillaries (Rosenberger *et al.*, 1993). Details of the X-ray topography investigations were given elsewhere (Stojanoff & Siddons, 1996; Stojanoff, Siddons, Monaco, Vekilov & Rosenberger, 1996). The topograph in Fig. 8 shows a 50–100 μm wide region of high strain in the center of the crystal. This region is larger than the core dimension estimated from the nucleation–growth–coring model, see §4, since strain fields always extend farther than the geometrical objects causing them. Such strained regions were only visible in some diffraction spots, presumably with a reflection vector yielding high contrast on interaction with an anisotropic strain tensor.

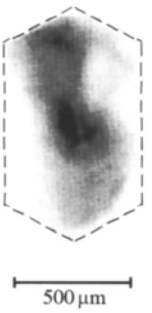

Fig. 8. Synchrotron monochromatic X-ray topograph of HEWL crystals. View perpendicular to the (110) face. Dark contrast at the center of the crystal indicates highly strained region.

Parallel determinations of X-ray diffraction resolution statistics revealed that crystals grown from Sigma solutions diffract to ~2.0 Å. Crystals grown from the purer Seikagaku solutions, that also exhibit lower ion content in core region (Fig. 6) diffracted to ~1.5 Å, the limit of the diffractometer used. Moreover, the latter crystals resulted in better signal-to-noise ratio, and displayed considerably lower mosaicity than crystals grown from Sigma solutions (Stojanoff *et al.*, 1996). This connection between coring and diffraction quality is not limited to lysozyme. Recently, Higuchi, Okamoto & Yasuoka (1995) performed local determinations of the diffraction resolution using a ~3.5 mm long hydrogenase crystal. They found that the diffraction resolution improved from >4 to ~2.5 Å with distance from the crystal origin.

Fig. 9 shows that in growth from Sigma solutions, the growth rates of small lysozyme crystals are considerably lower than those of larger ones. Size-independent growth rates were obtained only after the crystal dimensions reached about 100 μm. Note that this corresponds to the size of the strained region on Fig.

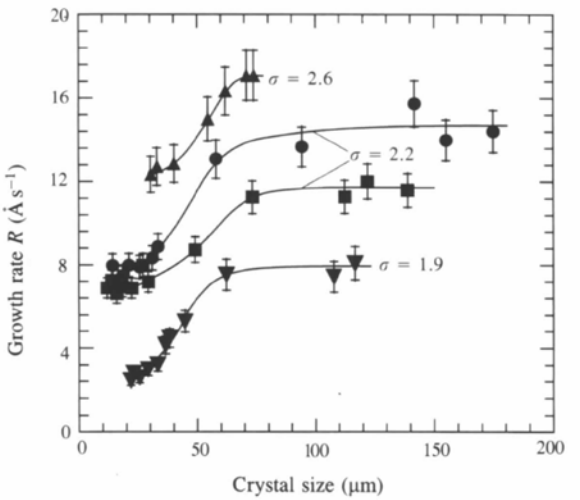

Fig. 9. Dependence of growth rate R on crystal size for crystals grown from Sigma solutions at various supersaturations. $C_{lys} = 50\,mg\,ml^{-1}$; supersaturation applied by lowering the temperature. Curves are just guides for the eye. Note that growth rate begins to accelerate at crystal sizes of ~30–40 μm. This size is roughly equal to that of the impurity/salt core (see §4.3). R reaches constant values at sizes ~80–100 μm, comparable to the size of the strained region in Fig. 8.

8. Similar observations of growth rate increase with crystal size abound in the mass crystallization literature (Ulrich & Kruse, 1990; Tulke & Offermann 1990; Zacher & Mersmann, 1995), where this phenomenon is studied to reduce unwanted growth rate dispersion. In investigation of individual crystals of sodium chlorate (Ristic, Sherwood & Wojciechowski, 1988, 1994), Rochelle salt (Mitrovic, 1994) and ammonium sulfate (Ó Meandra, Kramer & van Rosmalen, 1995), the lower growth rates of smaller crystals were correlated to their topographically determined higher strain densities. These were envisaged, in turn, to increase the solubility of the smaller crystals and, hence, to decrease the supersaturation and growth rate. It is also possible that the reduction in growth rate is caused by impurity effects on step kinetics (Vekilov & Rosenberger, 1996). Thus, the lower growth rate may not be a consequence of the higher strain, but an accompanying phenomenon with a common source - impurity adsorption and incorporation.

8. Summary and conclusions

We found that the precipitant ion incorporation into the crystals is not merely determined by crystallographic factors, or by molecular interactions in the solution. The ions are nonuniformly distributed within each crystal, and the initial and final amounts depend on the molecular ratio of precipitant to protein in the solution.

At small sizes ($\leq 40\,\mu m$), crystals capture higher precipitant and protein impurity concentrations than during their ensuing growth. This core causes lattice strain in the central crystal regions. This is also accompanied by a lower growth rate of core-sized crystals, as compared to larger ones.

Coring was not observed in crystallization from a highly purified solution.

We are grateful to R. M. Banish for help with the atomic absorption measurements, and to J. N. Sherwood, A. A. Chernov, M. Muschol and M. L. Pusey for helpful discussions. L. Carver prepared the figures. This work was supported by NSF (Grant No. DMB-9104630), NASA (Grant No. NAG8-950), and the State of Alabama through the Center for Microgravity and Materials Research at The University of Alabama in Huntsville.

APPENDIX

Depending on the specific physical conditions of a system, nucleation can be realistically described in terms of the simple classical approach or may require refined formulations in terms of modern statistical thermodynamic concepts or even atomistic approaches (for comparative discussions see Ruth, Hirth & Pound, 1988; Milchev, 1991). The choice of the appropriate formulation can be prompted by the number of molecules in a spherical critical nucleus i^*,

$$i^* = 4\pi r^{*3}/3\Omega = (4\pi/3\Omega)(2\Omega\gamma/\Delta\mu)^3 \simeq 32\pi\Omega^2\gamma^3/3(k_BT\sigma)^3, \quad (5)$$

where r^* is the radius of the critical nucleus, Ω is the volume per molecule in the crystal and γ the surface free energy. For lysozyme, $\Omega = 3 \times 10^{-20}\,cm^3$, and estimates for γ range from $0.4\,mJ\,m^{-2}$ (Chernov & Komatsu, 1995*b*) to $1.6\,mJ\,m^{-2}$ (Fiddis, Longman & Calvert, 1979). Using $\gamma = 1\,mJ\,m^{-2}$, for the highest $\sigma = 3.5$ employed, we get $r^* \simeq 40\,\text{Å}$ and $i^* \simeq 10$.

The classical approach has been shown to be adequate for critical nuclei containing more than 100 molecules (Lothe & Pound, 1962; Lee, Barker & Abraham, 1973). On the other hand, atomistic concepts are required when i^* is of the order of a few molecules (Stoyanov, 1974; Milchev, 1991). Therefore, we will use an approach based on statistical thermodynamics, taking advantage of a recent presentation by Mutaftschiev (1993). In this approach, translations and rotations of the critical cluster, that decrease its free energy, are taken into account (Lothe & Pound, 1962). We will consider the sequence monomer–dimer–trimer– ... –critical cluster–nucleus ..., rather than the more limited fluctuations approach of Volmer & Weber (1926). While we will not explicitly use a cluster-size-dependent surface energy (Tolman, 1949) in the derivations, such a dependence will be kept in mind when comparing model and experiment, since it could result in different γ's at different initial supersaturations.

*A*1. *Steady-state nucleation*

Since crystal nuclei result from collisions between critical clusters and monomers, the steady-state nucleation flux J_{st} (number of crystal nuclei per unit volume and unit time) is proportional to their respective concentrations z^* and n_1. As has been rigorously shown (for instance, Mutaftschiev, 1993),

$$J_{st} = k^* z^* n_1. \quad (6)$$

Here, k^* is a kinetic constant, proportional to the surface area of the critical cluster S^*, and the sticking coefficient κ. For solution growth, κ is similar in both its dependence on other parameters and its value to the step kinetic coefficients β_{step} (Chernov & Komatsu, 1995*a*), and is usually expressed as (Turnbull & Fisher, 1949; Walton, 1969; Kahlweit, 1969),

$$\kappa = a\nu^* \exp(-E_a/k_BT), \quad (7)$$

with a being the distance at which an approaching molecule feels the cluster. From recent estimates of interaction potentials between lysozyme molecules, based on light-scattering measurements (Muschol &

Rosenberger, 1995), $a \simeq 15$ Å. The ν^* in (7) is the frequency of attempts a monomer makes to stick to the cluster. Evaluating the expression (Glasstone, Laidler & Eyring, 1941),

$$\nu^* = (k_B T/2\pi m a^2)^{1/2}, \tag{8}$$

where $m = 2.4 \times 10^{-20}$ g is the lysozyme molecule mass, one obtains $\nu^* \simeq 3 \times 10^9\ s^{-1}$. In solutions of small molecules, ν^* is often estimated as $(k_B T/h)$, h being Planck's constant. This gives $\nu^* = 5.8 \times 10^{12}\ s^{-1}$ irrespective of molecular properties. Hence, (8), which was first used in protein crystallization by Chernov & Komatsu (1995*b*), seems a more realistic choice for the heavier protein molecules. Estimation of E_a in (7), the activation energy for attachment to the critical cluster, is difficult. Crystallization studies have shown that lysozyme growth is predominantly kinetics limited (Vekilov, Ataka & Katsura, 1993; Monaco & Rosenberger, 1993). Thus, in our case, E_a is likely closer to the activation energy for incorporation into the crystal rather than the often assumed activation energy for diffusion (Turnbull & Fisher, 1949). We assumed $E_a = 20\ kJ\ mol^{-1}$, which lies within the 12–25 kJ mol^{-1} range of earlier estimates (Vekilov, 1993; Chernov & Komatsu, 1995*b*).

Formulations for the steady-state concentration of critical clusters abound. It is generally agreed upon that (Zeldovich, 1942),

$$z^* = Z n^*, \tag{9}$$

where n^* is the constrained equilibrium concentration of critical clusters. Note that a true equilibrium state is possible only if the super-critical clusters (new phase) are not removed from the system, but are forced to decay to critical and sub-critical clusters. Hence, n^*, while useful for calculating z^* in (9), is devoid of physical reality. However, the relation of n^* to the monomer concentration n_1 has seen extensive conceptual controversy. By definition,

$$n^* = K n_1^{i^*}, \tag{10}$$

where K is the overall equilibrium constant between monomers and critical clusters, which can be expressed through the partition functions of these two species in the solution. This leads to (Mutaftschiev, 1993),

$$n^* = q_{rep} \exp(-\Delta G_{cl}^*/k_B T), \tag{11}$$

where $\Delta G_{cl}{}^*$ is the classical free enthalpy of the critical cluster,

$$\Delta G_{cl}^* = (16\pi/3)\ (\gamma^3 \Omega^2)/(k_B T \sigma)^2, \tag{12}$$

which accounts only for the energy gain due to the phase transition and the energy loss due to the creation of a new surface. The q_{rep} in (11) is the replacement partition function of the critical clusters per unit volume, which is the product of the translational and rotational configuration integrals of the cluster (Lothe & Pound, 1962). Its value can vary from 10^3 to 10^{25} (Lothe & Pound, 1969). These additional degrees of freedom of the cluster drastically enhance the nucleation rates over those predicted by the classical approach.

Instead of (11), following Frenkel (1946),

$$n^* = n_1 \exp(-\Delta G_{cl}^*/k_B T), \tag{13}$$

is often used (Walton, 1969; Kahlweit, 1969; Kashchiev, 1995). This 'Boltzman' or 'Gibbs' size distribution is intuitively appealing. However, since (13) implies $n^* \propto n_1^{(i^*+1)}$ (Lothe & Pound, 1969), it violates the mass action law, (10). This, as pointed out by Mutaftschiev (1993), is the result of a tacit error in the derivations of (13), involving the formulation of the thermodynamic potential of clusters.

Returning to (9), Z is the Zeldovich (1942) factor,

$$Z = (\Delta G_{cl}^*/3\pi k_B T i^{*2})^{1/2}. \tag{14}$$

Usually, Z is of the order 0.1 (Kashchiev, 1995) and, thus, results in substantially lower critical cluster concentration in steady state, than in constrained equilibrium. Z can be seen as effective width of the thermodynamic barrier for nucleation. As such, it accounts for slower formation not only of the i^*th, but also of (i^*-1)th, (i^*-2)th, ... clusters at the reduced supersaturations around the critical cluster.

Combining (5)–(9), (11), (12) and (14), we get for the steady-state nucleation flux,

$$J_{st} = 2\Omega(\gamma/\pi m)^{1/2} n_1 q_{rep} \exp(-E_a/k_B T) \times \exp[-16\Omega^2\gamma^3/3\pi(k_B T)^3\sigma^2], \tag{15}$$

i.e. a linear relation between J_{st} and monomer concentration n_1. This reflects the assumed formation of nuclei on collision of critical clusters with monomers. Note that on the use of the physically questionable (13) for the concentration of critical clusters (Kahlweit, 1969; Katz, 1970; Chernov, 1984; Malkin *et al.*, 1993), quadratic dependencies of J_{st} on n_1 follow. In comparisons with experimental data this conceptual flaw may remain undetected since n_1 (of order 10^{20}) can be close in order of magnitude to q_{rep}, (Katz & Ostermier, 1967; Katz, 1970). However, as was shown in §4.3, in protein solutions q_{rep} can be quite different from n_1 and thus unrealistic conclusions can result from this approach.

Yet other authors use (13) with a modified (6) in which J_{st} does not depend on n_1 (Walton, 1969; Kashchiev, 1995). Thus, the physically correct proportionality between J_{st} and n_1 is preserved for the wrong reasons.

A2. Time-dependent nucleation

Strictly speaking, steady state is possible in a nucleating system only if a constant source of monomers is present. Since our measurements were

performed in a closed solution volume, the applicability of the steady-state equations requires justification. The time-dependent nucleation flux $J_{ns}(t)$ is related to the steady-state J_{st} by (Kashchiev, 1969),

$$J_{ns}(t) = J_{st}\left[1 + \sum_{j=1}^{\infty}(-1)^j \exp(-j^2 t/\tau)\right], \qquad (16)$$

where,

$$\tau = 4/\pi^3 Z^2 k^* n_1, \qquad (17)$$

represents the nucleation induction period or time lag. Physically, τ is a measure of the time needed for the transformation of the initial cluster size distribution to the steady-state distribution (Kashchiev, 1995). Thus, if the characteristic time associated with significant concentration changes in the mother phase (due to nucleation and crystal growth) Δt is several τ, nucleation will follow the steady state (15). Using the above estimates of the spatial, temporal and energy factors, τ is of the order 0.1–1 s in our system. Since our observed Δt is several hours, the steady-state approximation applies to our data.

References

Ataka, M. & Asai, M. (1990). *Biophys. J.* **58**, 807–811.

Besho, Y., Ataka, M., Asai, M. & Katsura, T. (1994). *Biophys. J.* **66**, 310–313.

Blake, C. C. F., Koenig, D. F., Mair, G. A., North, A. C. T., Phillips, D. C. & Sarma, V. R. (1965). *Nature (London)*, **206**, 757–761.

Blake, C. C. F., Mair, G. A., North, A. C. T., Phillips, D. C. & Sarma, V. R. (1967). *Proc. R. Soc. London Ser. B*, **167**, 365–377.

Boistelle, R. & Astier, J. P. (1988). *J. Cryst. Growth*, **90**, 14–30.

Cacioppo, E. & Pusey, M. L. (1991). *J. Cryst. Crowth*, **114**, 286–292.

Chernov, A. A. (1984). *Modern Crystallography III: Growth of Crystals*. Berlin: Springer.

Chernov, A. A. & Komatsu, H. (1995*a*). In *Science and Technology of Crystal Growth*, edited by J. P. van der Eerden & O. S. L. Bruinsma, pp. 67–80. Dordrecht: Kluwer Academic Publishers.

Chernov, A. A. & Komatsu, H. (1995*b*). In *Science and Technology of Crystal Growth*, edited by J. P. van der Eerden & O. S. L. Bruinsma, pp. 329–353. Dordrecht: Kluwer Academic Publishers.

Elgersma, A. V., Ataka, M. & Katsura, T. (1992). *J. Cryst. Growth*, **122**, 31–40.

Feher, G. & Kam, Z. (1985). In *Methods in Enzymology*, Vol. 114, edited by H. W. Wykoff, C. H. W. Hirs & S. N. Timasheff, pp. 77–112. Orlando, Florida: Academic Press.

Fiddis, R. W., Longman, R. A. & Calvert, P. D (1979). *J. Chem. Soc. Faraday Trans. I*, **75**, 2753–2761.

Frenkel, J. (1946). *Kinetic Theory of Liquids*. Oxford University Press.

Frey, M. (1994). *Acta Cryst.* D**50**, 663–666.

Glasstone, S., Laidler, K. J. & Eyring, H. (1941). *The Theory of Rate Processes*. New York: McGraw Hill.

Higuchi, Y., Okamoto, T. & Yasuoka, N. (1995). Presentation Ps-13A-01 at Sixth International Conference on Crystallization of Biological Macromolecules, Hiroshima, Japan, November 1995.

Kahlweit, M. (1969). In *Physical Chemistry*, Vol. VII, edited by H. Eyring. New York: Academic Press.

Kam, Z., Shore, H. B. & Feher, G. (1978). *J. Mol. Biol.* **123**, 539–555.

Kashchiev, D. (1969). *Surf. Sci.* **14**, 209–220.

Kashchiev, D. (1995). *Science and Technology of Crystal Growth*, edited by J. P. van der Eerden & O. S. L. Bruinsma, pp. 53–66. Dordrecht: Kluwer Academic Publishers.

Katz, J. L. (1970). *J. Chem. Phys.* **52**, 4733–4748.

Katz, J. L. & Ostermier, B. J. (1967). *J. Chem. Phys.* **47**, 478–487.

Lee, J. K., Barker, J. A. & Abraham, F. F. (1973). *J. Chem. Phys.* **58**, 3166–3180.

Lothe, J. & Pound, G. M. (1962). *J. Chem. Phys.* **36**, 2080–2085.

Lothe, J. & Pound, G. M. (1969). *Nucleation*, edited by A. C. Zettlemoyer, pp. 109–149. New York: Marcel Decker.

Madhusudan, Kodandapani, R. & Vijayan, M. (1993). *Acta Cryst.* D**49**, 234–245.

Malkin, A. J., Cheung, J. & McPherson, A. (1993). *J. Cryst. Growth*, **126**, 544–554.

Malkin, A. J. & McPherson, A. (1993*a*). *J. Cryst. Growth*, **126**, 555–564.

Malkin, A. J. & McPherson, A. (1993*b*). *J. Cryst. Growth*, **128**, 1232–1235.

Malkin, A. J. & McPherson, A. (1994). *Acta Cryst.* D**50**, 385–395.

Milchev, A. (1991). *Contemp. Phys.* **32**, 231–332.

Mitrovic, M. M. (1994). *J. Cryst. Growth*, **139**, 332–335.

Monaco, L. A. & Rosenberger, F. (1993). *J. Cryst. Growth*, **129**, 465–484.

Muschol, M. & Rosenberger, F. (1995). *J. Chem. Phys.* **103**, 10424–10432.

Mutaftschiev, B. (1993). *Handbook of Crystal Growth. 1. Fundamentals*. Part A, *Thermodyanamis and Kinetics*, edited by D. T. J. Hurle, pp. 187–247. Amsterdam: North-Holland.

Nadarajah, A., Forsythe, E. L. & Pusey, M. L. (1995). *J. Cryst. Growth*, **151**, 163–172.

Narang, R. S., Sherwood, J. N., Cliff, M. J. & Jones, H. A. (1978). *Inst. Chem. Eng. Symp. Ser.* **54**, 267–277.

Niimura, N., Minezaki, Y., Ataka, M. & Katsura, T. (1994). *J. Cryst. Growth*, **137**, 671–675.

Ó Meandra, R. S., Kramer, H. J. M. & van Rosmalen, G. M. (1995). *J. Cryst. Growth*, **152**, 314–320.

Pusey, M. L. (1992). *J. Cryst. Growth*, **122**, 1–7.

Ristic, R. I., Sherwood, J. N. & Wojciechowski, K. (1988). *J. Cryst. Growth*, **91**, 163–168.

Ristic, R. I., Sherwood, J. N. & Wojciechowski, K. (1994). *J. Cryst. Growth*, **144**, 87–90.

Roberts, K. J., Sherwood, J. N. & Stewart, A. (1990). *J. Cryst. Crowth*, **102**, 419–426.

Rosenberger, F. (1986). *J. Cryst. Growth*, **76**, 618–636.

Rosenberger, F., Howard, S. B, Sowers, J. W. & Nyce, T. A. (1993). *J. Cryst. Growth,* **129**, 1-12.

Rosenberger, F., Vekilov, P. G., Muschol, M. & Thomas, B. R. (1996). *J. Cryst. Growth*. In the press.

Roxby, R. & Tanford, C. (1971). *Biochemistry*, **10**, 3348-3352.

Ruth, V., Hirth, J. P. & Pound, G. M. (1988). *J. Chem. Phys.* **88**, 7079-7087.

Sibille, L. & Pusey, M. L. (1994). *Acta Cryst.* D**50**, 396-397.

Sophianopoulos, A. J., Rhodes, C. K., Holcomb, D. N. & Van Holde, K. E. (1962). *J. Biol. Chem.* **237**, 1107-1112.

Stojanoff, V. & Siddons, D. P. (1996). *Acta Cryst.* A**52**, 498-499.

Stojanoff, V., Siddons, D. P., Monaco, L. A., Vekilov, P. G. & Rosenberger, F. (1996). In preparation.

Stoyanov, S. (1974). *Thin Solid Films*, **18**, 91-98.

Tanford, C. (1962). *Advan. Protein Chem.* **17**, 69-165.

Tanford, C. & Wagner, M. L. (1954). *J. Am. Chem. Soc.* **76**, 3331-3336.

Thomas, B. R. Vekilov, P. G. & Rosenberger, R. (1996). *Acta Cryst.* D**52**, 776-784.

Tolman, R. C. (1949). *J. Chem. Phys.* **16**, 758-774.

Tulke, A. & Offermann, H. (1990). In *Proceedings 11th Symposium Industrial Crystallization*, Garmisch-Partenkirchen, Germany, edited by A. Mersmann, pp. 441-446.

Turnbull, D. & Fisher, J. C. (1949). *J. Chem. Phys.* **17**, 71-73.

Ulrich, J. & Kruse, M. (1990). In *Proceedings 11th Symposium Industrial Crystallization*, Garmisch-Partenkirchen, Germany, edited by A. Mersmann, pp. 361-366.

Vekilov. P. G. (1993). In *Studies and Concepts in Crystals Growth*, edited by H. Komatsu, pp. 25-49. Oxford: Pergamon Press.

Vekilov, P. G., Ataka, M. & Katsura, T. (1993). *J. Cryst. Growth*, **130**, 317-320.

Vekilov, P. G., Ataka, M. & Katsura, T. (1995). *Acta Cryst.* D**51**, 207-219.

Vekilov, P. G., Monaco, L. A. & Rosenberger, F. (1995). *J. Cryst. Growth,* **156**, 267-278.

Vekilov, P. G. & Rosenberger, F. (1996). *J. Cryst. Growth,* **158**, 540-551.

Volmer, M. & Weber, A. (1926). *Z. Phys. Chem. (Leipzig)*, **119**, 277-301.

Walton, A. G. (1969). In *Nucleation*, edited by A. C. Zettlemoyer, pp. 225-307. New York: Marcel Decker.

Wilson, L. J. & Pusey, M. L. (1992). *J. Cryst. Growth*, **122**, 8-13.

Zacher, U. & Mersmann, A. (1995). *J. Cryst. Growth,* **147**, 172-180.

Zeldovich, Y. B. (1942). *J. Exp. Theoret. Phys. (USSR)*, **12**, 525-538.